Solar Energy 295 (2025) 113526

Contents lists available at ScienceDirect

Solar Energy

journal homepage: www.elsevier.com/locate/solener

Loop-wise control valves application in molten salt parabolic trough solar fields

Tim Kotzab [a,*], Sebastian Müllner [a], Jana Stengler [a], Bijan Nouri [b], Luis Fernando Zarzalejo [c], Mark Schmitz [d], Tobias Hirsch [a]

[a] German Aerospace Center (DLR), Institute of Solar Research, Wankelstraße 5, 70563 Stuttgart, Germany
[b] German Aerospace Center (DLR), Institute of Solar Research, Ctra de Senes s/n km 4, 04200 Tabernas, Spain
[c] CIEMAT Energy Department – Renewable Energy Division, Av. Complutense 40, 28040 Madrid, Spain
[d] TSK Flagsol Engineering GmbH, Anna-Schneider-Steig 10, 50678 Cologne, Germany

A R T I C L E I N F O

Keywords:
Parabolic trough power plant
Solar field control
Control valves
Molten salt
Virtual solar field

A B S T R A C T

Parabolic trough power plants use collectors to concentrate direct sunlight onto an absorber tube containing a heat transfer fluid (HTF). The thermal energy is used to generate electricity in a steam cycle power plant. In almost all commercial power plant designs, the HTF is distributed homogeneously to all loops with a fixed opening for the manual loop inlet valves. This work presents an approach with individually controlled mass flow distribution to all loops. The objective is to achieve a more stable outlet temperature in the event of non-homogeneous irradiation. The control concept includes a controller for the total mass flow at the HTF pump, the focus rate of each collector and the opening of the individual loop inlet valves.

The suggested control concept is tested using the Virtual Solar Field (VSF) dynamic simulation tool for a 38-loop molten salt parabolic trough field. This simulation tool uses highly discretized irradiance data to reproduce realistic irradiance boundary conditions. A total data set of 940 days of operation recorded at CIEMAT's Plataforma Solar de Almería are used. Furthermore, different artificial soiling scenarios are implemented to test the concept under non-homogenous heat input. The new control concept is compared with the state-of-the-art control schemes based on loop inlet valves with fixed opening. For normal soiling conditions, the simulation results show an average increase of 0.85 % in the net electrical energy produced.

1. Introduction

Concentrated solar power (CSP) systems are used to generate thermal and electrical energy from solar radiation. By the end of 2020, 6.5 GW of capacity have been installed worldwide, representing 0.23 % of total renewable energy capacity [1]. To generate thermal energy, the direct normal irradiance (DNI) of the sun's rays is first concentrated to heat up a heat transfer fluid (HTF). The solar radiation can be concentrated on a line or on a point focus. Point concentrating systems are solar towers with multiple heliostats that focus the irradiance onto the top of a receiver tower. Line concentrating systems apply either Fresnel or parabolic trough (PT) collectors to focus the sun's rays onto a receiver tube. After being heated in the solar system, the hot HTF passes through a heat exchanger to produce superheated steam, which is used to generate electrical power through a conventional Rankine cycle turbine. Most commercial PT plants use a thermal oil as the HTF and have a typical capacity of 50 MW_{el} [2]. This paper deals with the control of the solar field (SF) of a PT power plant with molten salt as heat transfer fluid.

Parabolic trough field setup.

The SF is usually divided into several sub-fields with approximately the same number of loops. A loop consists of several solar collector assemblies (SCAs), each one moved by a separate drive to track the position of the sun. The mass flow of the HTF is provided by a central pump for the whole SF and is distributed homogeneously by manual valves located at the entry to each loop. Despite minor adjustments to improve the hydraulic balance, the loop valves' positioners remain unchanged during operation. The balancing is usually carried out several times a year to compensate for seasonal variations in the average thermal load on the SF. Only a few parabolic trough plants, such as the Lebrija 1 [3] plant in Spain, are equipped with automatic control valves in the loops. These control valves can adjust the mass flow of each loop according to the cloud situation.

* Corresponding author.
E-mail address: tim.kotzab@dlr.de (T. Kotzab).

https://doi.org/10.1016/j.solener.2025.113526
Received 20 December 2024; Received in revised form 28 March 2025; Accepted 15 April 2025
Available online 28 April 2025
0038-092X/

Nomenclature

ASI	all sky imager
c_p	Specific heat capacity
CSP	concentrated solar power
DNI	direct normal irradiance
e	control error
E_{net}	electrical energy
f	focus
f_c	sensitivity factor of controller
HTF	heat transfer fluid
K	gain factor
$\dot{m}$	mass flow
MPC	model-predictive control
P	power consumption
p	pressure
PID	proportional-integral-derivative
PSA	Plataforma Solar de Almería
PT	parabolic trough
Q	volumetric flowrate
$\dot{Q}$	heat flow
s	valve opening
SCA	solar collector assembly
SF	solar field
T	temperature
T_p	time constant
$\dot{V}$	volume flow
VSF	virtual solar field
y	control output

Greek Symbols

α	SCA angle
η	efficiency
θ	deadtime
ρ	density

Subscripts

base	base opening of valve
i	number of loop
in	inlet of SF
loop	loop number
max	maximum
min	minimum
out	outlet of SF
PB	power block
set	setpoint
v	valve number

An expected improvement from valve control is the individual adjustment of the mass flow in each loop to its specific heating conditions. Individual heating conditions are induced by inhomogeneities in solar radiation, typically caused by clouds passing over the field, and inhomogeneities in the soiling of the SCAs on the field. At ideal loop mass flow, the loop outlet temperature approaches its setpoint and the collectors are fully in focus. A high HTF outlet temperature of the SF improves the power cycle efficiency as well as the utilization of the installed storage capacity by charging the storage with the full temperature difference.

Molten salt as heat transfer fluid in parabolic trough field.

In this study, a direct molten salt PT field is used instead of a system with thermal oil as HTF. Line focusing systems using molten salt are still under development, with only a few plants in operation, e.g. the plant in Archimede [4] in Italy. The motivation for using molten salt is the increased SF outlet temperature of 500 to 550 °C and the reduced pumping power resulting from advantageous fluid properties of molten salt. The significant temperature increase of 200 to 250 K between the inlet and outlet of the SF, compared to the small temperature difference of 80 to 100 K that is typical for oil-based systems, results in more efficient thermal storage. The optimal loop length for molten salt fields (∼800–1000 m per loop) is larger than for oil fields (∼600 m per loop). This reduces the number of loops and the number of controlled loop inlet valves in the field. The additional investment in controlled motor valves is therefore lower than for oil-based fields helping to improve economics of the additional investment. Although analyzed for molten salt systems in this paper, the general findings of the molten salt control concept investigated in this paper can be transferred to oil-based systems.

Literature overview.

An overview of control schemes for parabolic trough fields is given in [5] and [6]. Most commercial-scale plants use traditional proportional-integral-derivative (PID) feedback controllers [7]. Feedforward controllers can be used in addition to correct for measurable external effects like the continuous change of the DNI level, which is typically measured by pyrheliometers at a few points in the SF [8]. Recent research work introduced control approaches utilizing all sky imagers (ASI) to obtain a spatially resolved DNI map over the SF [9,10,11,12]. The principle behind this approach is to use the additional information from the measurement in a feed-forward or model-predictive control (MPC) approach to reach better controller performance. A number of advanced control concepts like gain scheduling [13], MPC [14], fuzzy logic control [15] or neural network controllers [16] have been developed but, to the knowledge of the authors, have not been applied in commercial plants. Nearly all of these control concepts are designed for solar fields with non-controlled loop inlet valves.

In [17], temperature homogenization with control valves is studied: the study is based on the ACUREX SF, a former test field with 10 loops at CIEMAT's Plataforma Solar de Almería (PSA). A test duration of approximately 7.5 h was carried out with a feed-forward controller in comparison to a MPC. The SF with the MPC can generate 3.3 % up to 4.4 % more depending on the soiling conditions in the field. The study has some limitations since the MPC concept is compared with a feed-forward control which by default has no feedback part to consider current situations. The authors state an advantage due to the control valves although the reported benefits are probably too optimistic. The same authors published a case study on larger PT plants [18], concluding that the number of defocusing actions can be reduced to almost one-tenth for stable radiation or prevented completely for transient radiation by using control valves for a 50 MW power plant with 90 loops. But again, an MPC controller is compared to a feed-forward control.

A comparison between motorized and manual valves on the performance during short cloud shading is reported in [19]. A dynamic cloud shading model was used to create four different artificial cloud shading patterns for a SF size of 1.2 x 1.2 km^2 with 100 loops and up to 250 s simulation time. The analysis indicates that there is almost no difference in net energy generation between the motorized and manual valves setup. However, it was possible to keep the temperature almost at a stable value with the motorized controller, whereas the temperature dropped up to 10 K with the manual valves.

The results presented in Paper [20] demonstrate a 1.09 % enhancement in the generated thermal power for an MPC with control valves, in comparison to an MPC with manual valves, for the configuration of the ACUREX SF test field. For the case study, a two-hour synthetic DNI profile was used. An artificial cloud has been simulated in the DNI profile for a period of 15 min. The aim of the control was to maximize the thermal output without any particular need to achieve a stable outlet temperature [21]. However, evaluating the generated thermal output alone, and neglecting temperature stability is a simplification that does not represent the operation of a commercial CSP system: any drop in the field outlet temperature will have a direct impact on the temperature entering the power cycle and therefore reduce its efficiency. In addition, the effective storage capacity is reduced as the design temperature difference is not fully utilized. [22] repeated the study for an upscaled ACUREX SF of 100 loops with a MPC controller. The authors describe a maximum improvement of 1.10 % in thermal performance for the MPC against the controller with no control valves.

Compared to the previous papers, the present work aims at providing a more holistic view of the irradiance situations considered. The investigated change in net electricity generation is evaluated for a number of 940 operation days recorded at CIEMAT's PSA within a three-year period. For these days, spatially and temporally resolved irradiance data from an ASI system are available, resulting in a highly realistic representation of the irradiance situation. The real irradiation data can be used in combination with the VSF tool to perform dynamic and transient simulations. VSF utilizes spatially resolved irradiation maps to calculate an individual DNI value for each collector. This facilitates the simulation of real dynamic situations with VSF and the development of control concepts. Furthermore, various soiling scenarios are developed that can be simulated with VSF. Consequently, the novel control concept developed in the paper can be developed and tested in real situations. We rely on traditional control elements based on feed-forward and PID feedback loops, which are more readily accepted by the power plant industry. A reference control case without individual loop control is defined to explicitly work out the differences induced by the controlled valves. The final evaluation considers several criteria such as the focus rate, the number of overtemperature defocusing events, the temperature stability and the thermal power. Subsection 2.1 explains the calculation of the DNI maps and the detailed simulation model of the SF. The design of the fixed valve control and the individual valve control is described in subsection 2.2. The performance indicators and soiling scenarios for evaluation are defined in subsection 2.3 and the simulation results are analyzed in section 3.

2. Methods

To evaluate the control valves, spatially and temporally resolved DNI maps are used in the Virtual Solar Field (VSF) simulation tool. Individual valve control is compared to manual valves with a fixed valve opening by evaluating the net electrical energy generated at different soiling scenarios.

2.1. Boundary conditions and plant setup

The DNI maps are based on a record of cloud cameras. The layout of the SF with the control valves is integrated and tested in the simulation environment.

Pre-processing of the DNI maps as input to the simulation

The spatial and temporal resolved DNI maps are derived from an ASI system, which is operated at CIEMAT'S PSA. The upward facing cameras with fisheye lenses are taking a picture every 30 s to detect clouds in the sky [23]. The shadows of the clouds are projected on the surface via a raytracing algorithm. By the combination with the cloud transmittance, a spatial map is derived. A detailed description of the process can be found in [24,25,26]. From this highly resolved map, an average DNI value of each SCA is determined in each time step and applied as heat input in the simulation tool.

For this study, 1,063 days from 2016, 2017 and 2018 have been processed in the period between 9:00 to 18:00. Some few days could not be recorded due to system failures. Since not each day is qualified for the operation of a solar power plant, unsuitable ones were discarded. Periods with solar elevation angle of more than 12° are used in order to cover also the complete startup and the begin of the shutdown of the SF. The remaining 940 days with a total simulation time of 7,222 h are shown in Fig. 1 with the average DNI over the day and the usable time period.

Virtual Solar Field simulation model.

The simulation tool Virtual Solar was developed at the Institute of Solar Research at German Aerospace Center and is described in detail in [27]. It combines hydraulic, like the mass flow depending on the pressure losses, and thermal calculations, like the temperature losses and gains, of the HTF in the SF. The modelling of each pipe starts at the pump and the cold header to the subfields with the loops and ends at the hot header at the power block. The layout of the SF can be set individually by determining the position of each pipe and SCA. It is possible, to set an individual DNI value for each SCA every two seconds. The tool was successfully validated against a commercial power plant [28].

An artificial SF layout with two subfields is implemented for this study. Each subfield contains 19 loops, each with 4 HelioTrough SCAs. The HelioTrough has a length of 191 m and a aperture width of 6.78 m [29] and is equipped with a PTR®90 absorber tube for molten salts. In the present simulation, the acceptance angle curve for the SCAs was used in accordance with the curve shown in [28]. The nominal DNI is set to 800 W/m^2. In the present study, the SolarSalt is analyzed as a molten salt. Properties for salt and receiver are shown in Table 1. The nominal outlet temperature is 505 °C. The product is suitable for use in a 480 °C industrial turbine. The nominal field inlet temperature is 290 °C. The heat exchanger and Rankine cycle gross power is 50 MW$_{el}$. The operation strategy implemented includes the start-up of the SF (completed as soon as the threshold of 500 °C is reached at outlet) and the normal operation. SF shutdown and night mode are not included in the simulation since the benefit from the individual valve control are expected to be minor in this operation regime.

Special care was taken for the definition and modeling of the control valves. In absence of commercially established standards on control valves for molten salt, this study considers a proportional behavior between the opening of the valve and the flow factor K_v. Valves with a maximum flow factor of 20 m^3/h at each loop are implemented. This value is a compromise between a moderate pump pressure of the HTF main pump and a high control range of individual mass flow in the loops. The valve induces a pressure loss (Equation (1) to the hydraulic network where Q is the volumetric flowrate and ρ the density of the HTF.

$$\Delta p_i = \left(\frac{Q}{K_v}\right)^2 \bullet \frac{\rho}{1000\,\frac{\mathrm{kg}}{\mathrm{m}^3}} \bullet 1\mathrm{bar} \tag{1}$$

The mean valve opening over all valves for a homogenous mass flow distribution in the SF is set to 40 %, whereas the minimum allowed valve opening is 20 %, and the maximum 100 %. The resulting mass flow control ranges are shown in Fig. 2 for a DNI level of 400 W/m^2 and 800 W/m^2, respectively. The graph shows the range of possible mass flow that can be reached by opening (up to 100 %) and closing (down to 20 %) one single valve while the others remain at their nominal opening of around 40 %. The behavior is within ± 10 % at low DNI and ± 30 % at high DNI. It can also be seen, that the individual control range gets smaller for loops farther away from the field inlet. This effect is caused by the slightly different nominal valve opening that has to compensate individual pressure difference across the loop which depends on the position in the header. The outer loops have a slightly larger opening than the SF mean value of 40 % to compensate for pressure losses in the header lines. The results shown Fig. 2 are obtained from the VSF simulation. Any opening or closing of a single valve also slightly impacts the flow in the other loops. The diagram clearly shows that even with the controlled valves, it is not possible to adjust the mass flow in a loop to any desired value. A larger control range would be possible if the nominal pressure loss over the valves was increased. Since this impacts the overall pressure loss in the field and thus the required pumping power the chosen setup is considered to be a good trade-off.

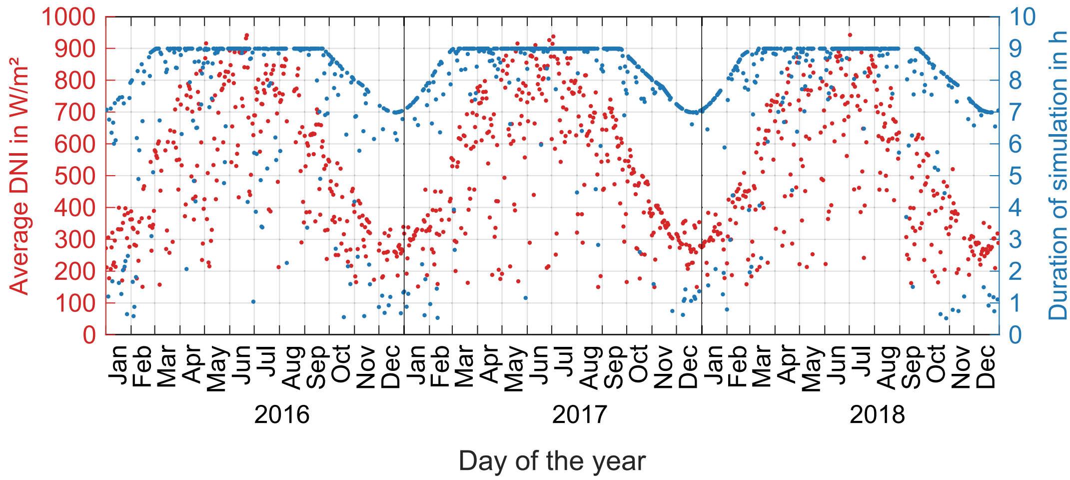

Fig. 1. Daily average DNI and usable time period of 2016, 2017 and 2018. Maximum time of 9 h given by existing data.

Table 1
Properties of molten salt and receiver.

Density SolarSalt $\left[\frac{kg}{m3}\right]$	$\rho = 2194.6 - 0.6681 \cdot T$
Heat Capacity SolarSalt $\left[\frac{kJ}{kg \cdot K}\right]$	$cp = 1.5133 + 0.0002 \cdot T$
Heat Conductivity SolarSalt $\left[\frac{W}{m \cdot K}\right]$	$\lambda = 0.5108 + 9e^{-5} \cdot T - 5e^{-7} \cdot T^2$
Thermal Losses Absorber PTR 90 $\left[\frac{W}{m}\right]$	$q_{loss} = 2.7e^{-7} \cdot T^4 - 0.0004 \cdot T^3 + 0.2503 \cdot T^2 - 65.3730 \cdot T + 6377.6587$

2.2. Controller setup

As the literature review revealed, there is a wide variety of control strategies for the SF, typically distinguishing between operation modes startup, normal operation, shutdown, recirculation, and night mode. The here described controllers are intentionally designed for the normal operation but other operation modes are possible with a few modifications. For this reason, it is assumed that the normal operation mode concept can be applied as soon as the DNI reaches a threshold of 300 W/m^2. This DNI value is necessary to reach the nominal outlet temperature of 505 °C given the defined minimum loop mass flow of 2.81 kg/s in the loop. Control elements based on feed-forward using DNI measurements as described e.g. in [10,12] are not used for this study.

In general, the fixed and the individual valve control are both based on the principle of a primary/secondary control scheme. The primary controller(s) uses the measured temperatures of the loops to calculate the control output (SCAs focus or valve opening). The secondary controller(s) uses the control output of the primary controller as an input and generates the mass flow control output for the HTF pump. This method neglects interferences between the controllers by connecting them in series. All controllers are designed to work with deviations from a base value rather than absolute values. This leads to a smoother start of the system and can better be adjusted to the control range. All PI-controllers are equipped with an anti-windup logic in order to prevent the overflow of the integral part. The fixed and the individual valve control are described in the following. Afterwards the approached used for identification of the control parameters is specified and some additional functions of the control are outlined. The equations for the PI controllers are shown in the control parameters section and the steps for calculating the individual parameters are explained. In this context, the ranges in which the parameters of the individual controllers lie are specified.

Fixed valve control.

In commercial PT power plants, the individual loop temperature is controlled by controlling the tracking position, namely the deviation of the tracking position relative to the theoretical tracking position of the SCAs. In addition, the mass flow to the whole field is controlled to avoid significant defocusing of collectors. The reference control system in this study follows this approach. A basic opening is selected for the valve

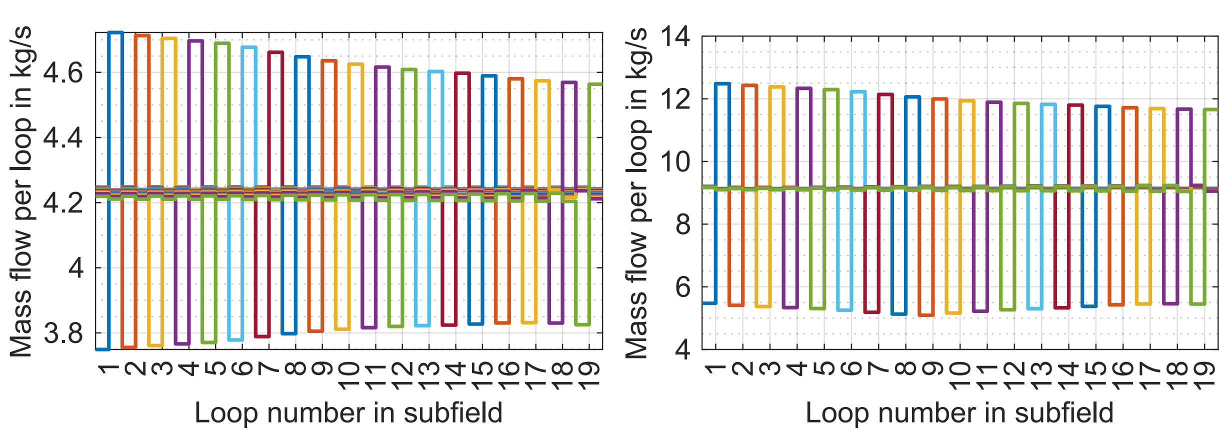

Fig. 2. Operational range of loop mass flows based on loop wise opening and closing of the control valves within the defined limits of 20 % … 100 % at a DNI of 400 W/m^2 (left) and 800 W/m^2 (right). The diagram shows the resulting mass flow when closing the valve in loop i (lower mass flow value) and fully opening the valve (higher mass flow value).

opening, which is 40 % on average for all valves. Thus, an almost equal mass flow will be available in each loop during the simulation.

A scheme of the developed control is shown in Fig. 3. In this approach, only the last SCA in each loop is directly controlled. The base focus f_{base} is set to 100 % and the saturation has a minimum $f_{min} = 0$ % and a maximum$f_{max} = 100$ %. For the mass flow controller, the task is to adjust the total mass flow rate of the HTF into the whole solar field in a way that the average deviation of the focus of all controlled SCAs is 0 %, which corresponds to a total focus rate of 100 %. This procedure assures that a high outlet temperature at maximum possible mass flow is reached. The average value of all focus controllers is calculated and used as input for the mass flow controller. In the sum block, all values are added up and divided by the number of loops. The minimum mass flow for the SF inlet $\dot{m}_{min}$ is defined by the minimal mass flow per loop multiplied by the number of loops. The upper limit $\dot{m}_{max}$ set to 350 kg/s. This value can be set situation-based, e.g. on the filling level of the TES, but in this study, it is assumed static. The base mass flow $\dot{m}_{base}$ is set to 190 kg/s.

Individual valve control.

For the individual valve control, the primary controllers are the valve controllers, as shown in the control scheme in Fig. 4. The individual valve opening is controlled by the outlet temperature of the loop. The base valve opening of the i-th loop $s_{V,base,i}$ is the opening that results in a homogeneous mass flow distribution over the SF with a mean opening of 40 %. In our case, the base valve opening ranges from 36 % to 43 % with the lower values found at the inner loops. The mass flow controller takes the valve openings from the valve controller and controls the mass flow in a way that the mean valve opening comes back to its design value of 40 %. The function and limits of the mass flow controller are similar to the fixed valve control. The focus controllers do not have an integral component due to the compensation of the control error in the valve controllers and the direct impact without any delay onto the focus. Their control errors are determined by the difference to the maximum opening of the valves to achieve that the focus is only reduced when the valves would come out of the control range. The limits f_{min} and f_{max} are identical with the fixed valve control. Consequently, the focus controller only becomes active when the maximum valve opening from the valve controller is exceeded. Subsequently, the focus controller will reduce the focusing of the SCA to prevent the temperature from being exceeded.

Control parameters.

The parameters of the controllers are tuned using the first-order plus dead time method, as previously investigated in [27]. This allows the identification of the control values by analyzing the controlled system, here the SF. To calculate the proportional gain factor (Equation (2) the proportional gain factor K_p, the time constant T_p and the deadtime θ_p of the SF and a factor f_c used to determine the sensitivity of the controller is needed.

$$K_c = \frac{1}{K_p}\frac{T_p}{\theta_p + f_c \bullet T_p} \tag{2}$$

By the multiplication with the control error $e(t)$ the control output (Equation (3) can be calculated.

$$y(t) = K_c \bullet e(t) + \frac{K_c}{T_p}\int e(t)dt \tag{3}$$

In order to determine the parameters of the SF, multiple step responses like shown in Fig. 5 are simulated. To tune the system some basic controllers with estimated parameters are applied in VSF. After the settling of the system the basic controllers are turned off and a DNI step is applied. Thereby the temperature difference per loop ΔT and the time constant T_p, which occurs at 63 % of the temperature difference ΔT, is identified. By activating the valve controllers, the change of the opening of the valves Δs_V can be measured and the proportional gain (Equation (4) of the valves can be calculated.

$$K_{p,valve} = \frac{\Delta s_V}{\Delta T} \tag{4}$$

By activating the mass flow controller, the proportional gain (Equation (5) of the mass flow can be determined by the ratio of the change of the mass flow $\Delta\dot{m}$ and the change of the average valve opening $\Delta s_{V,avg}$.

$$K_{p,pump} = \frac{\Delta\dot{m}}{\Delta s_{V,avg}} \tag{5}$$

The step response is evaluated at a DNI of 600 W/m^2 resulting in a range of the proportional factor of the valves $K_{p,valve}$ between 25 %/K and 42 %/K and a time constant T_p of 700 s. The sample time for each individual controller is set to 10 s, and the dead time is configured to match this value, thus also being 10 s. The configuration of the controller dead time was adjusted so that it corresponds to the value of the sample time as evaluated in the reference [27].

The gain of the mass flow controller is set to −0.0026 kg/(s %) and of the focus controller is calculated with Equation (6), where ΔT_{coll} represents the temperature difference reached in the last SCA and is estimated to 50 K, α_{max} is the angle necessary for a complete defocus and $K_{c,valve}$ the proportional factor of the valve controller. The sensitivity factor f_c is tuned to a value of 0.3 for the PI controllers.

$$K_{p,focus} = \frac{\Delta T_{coll}}{\alpha_{max}} \bullet K_{c,valve} \tag{6}$$

To determine the control parameters for the fixed valve control a conversion is used. The proportional factor for the focus control is set with Equation (7) and for the mass flow controller with Equation (8).

$$K_{p,focus,fix} = K_{p,valve} \bullet K_{p,focus} \tag{7}$$

$$K_{p,pump,fix} = \text{mean}\left(\frac{K_{p,pump}}{K_{p,focus}}\right) \tag{8}$$

The time constant T_p and the dead time θ_p is the same as in the individual valve control (10 s), whereas the individual tuning resulted in a higher

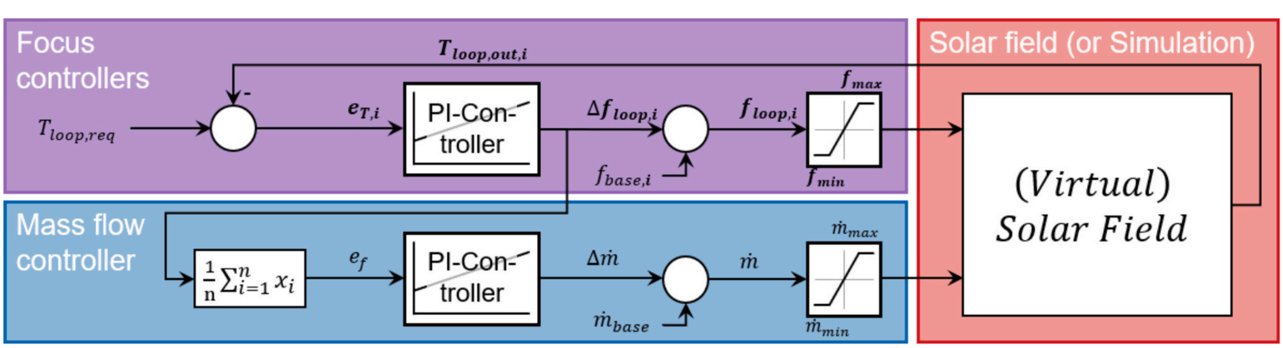

Fig. 3. Control scheme of the fixed valve control.

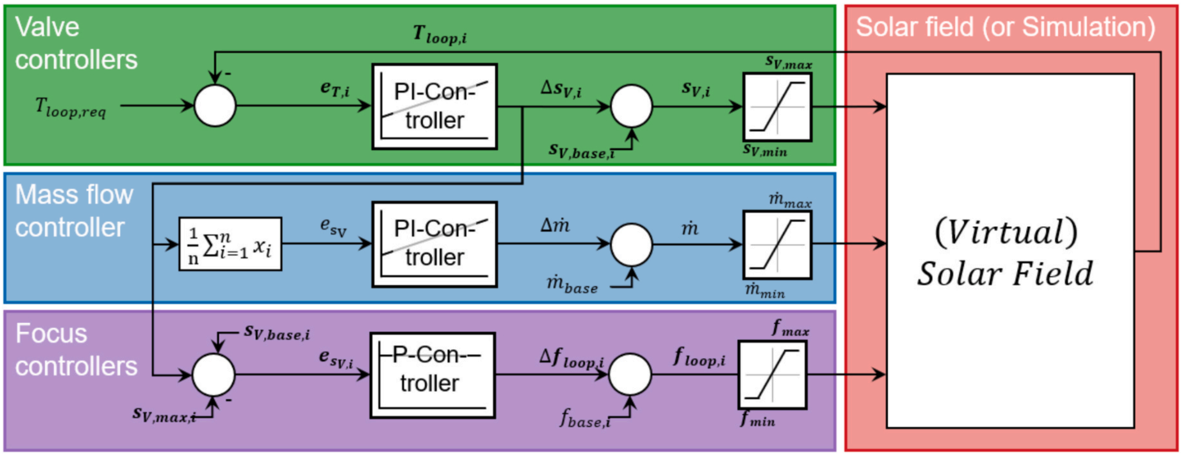

Fig. 4. Control scheme of the individual valve control.

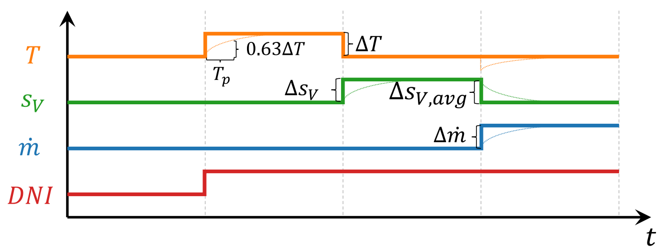

Fig. 5. Schematic for the step response for parameter detection.

sensitivity with the factor $f_c = 0.15$.

Additional control functions.

To guarantee the safety of the SF operation, some more functionalities are needed. Since the focus controller acts only on the last SCA in the loop, any previous SCAs in the line must reduce its focus if its individual SCA outlet temperature exceeds a safety threshold. In the given setup, the temperature is only measured in the middle of the SCA. The outlet temperature of each collector is calculated as the mean value of the current and the following collector. A temperature transition area is defined to avoid immediate change between full and no focus as illustrated for the third SCA in Fig. 6. The graphic shows that the track deviation angle of the SCA changes linear, whereas the effective focus rate is non-linear. The temperature thresholds for a full defocus are set to 410 °C, 460 °C, 485 °C, 505 °C and 510 °C for the first end, second end, third end, last middle and last end SCA temperature.

A minimum mass flow guaranteeing turbulent conditions has to be maintained in each loop. For the fixed valve control this is applied by the minimal total mass flow in combination with the homogenous mass flow distribution to all loops. The tolerated openings of the valves (20 % … 100 %) are additionally reduced when the actual mass flow approaches the minimum mass flow limit. The so corrected minimum and maximum allowed valve openings for the last valve of the subfield are shown in Fig. 7. Here the limitation starts at a value of $\dot{m}_{in} = 1.5\dot{m}_{min}$ and prohibits a valve opening change at a value of $\dot{m}_{in} =< 1.15\dot{m}_{min}$.

Temperature overshoots at the loop outlet are considered as very critical since they can cause damage to components or degradation in the HTF. To further suppress any temperature overshoots, the temperature control deviation e_T is amplified with a nonlinear correction as soon as the threshold temperature of 500 °C is exceeded. The correction faction also depends on the valve opening. The way of modifying the control error instead of adapting the controller parameters themselves has the advantage of a faster changing integral and therefore a faster adjustment of the whole control. The resulting corrected control error e_T depending on the loop outlet temperature is shown in Fig. 8. It can be seen, that the temperature error is three to nine times higher for a temperature excess as is for a undershoot.

Another boundary condition to be satisfied are temperature gradients over time. A maximum temperature gradient of 5 K/min has to be guaranteed at the SF outlet in order to avoid temperature shocks in the downstream headers. In situations after longer shading periods, a sudden increase in irradiance can lead to high gradients. A trajectory controller is added to take care for the gradients. Fig. 9 shows an

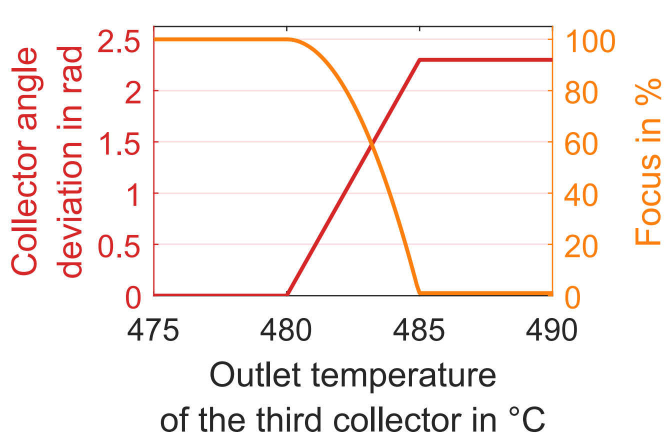

Fig. 6. Overheat protection by defocusing for the third SCA.

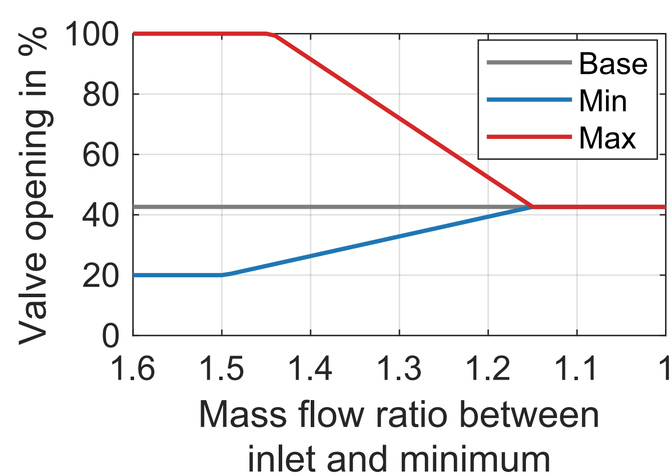

Fig. 7. Limitation of the tolerated valve openings when approaching the minimum mass flow limit (Example for the last loop in the sub-field).

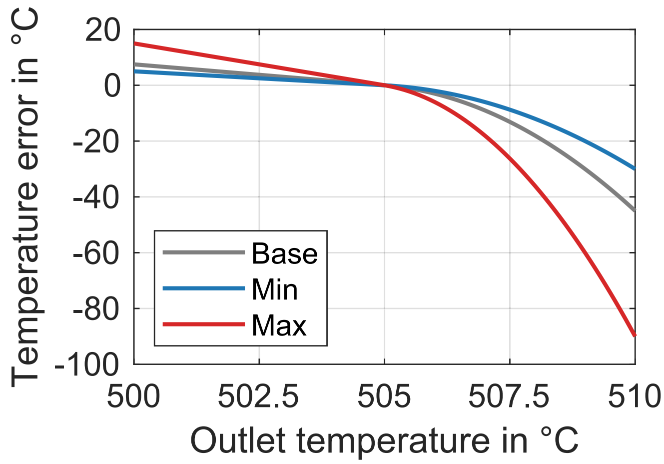

Fig. 8. Temperature error amplification for three different valve openings (min, base, max).

example simulation of how this concept works during a start-up situation. The temperature set-point is at its default value of 505 °C. At simulation time ~ 1 min (temperature gradient is higher than 5 K/min), the temperature setpoint T_{set} switches to the current temperature and is increasing with the highest allowed temperature gradient (5 K/min). This reduces the gradient and keeps it at the 5 K/min as far as possible.

2.3. Evaluation methodology

The potential net generated electrical energy is used as key performance indicator to compare the valve control with the fixed valve control concept. Since the simulation itself is done only for the solar field, the impact on the power block is calculated by simplified models which are explained in the following. The impact on storage utilization by stabilized field outlet temperature is not considered in this study. Approaches for this aspect are e.g. published by [28].

Performance indicators.

The basis for the evaluation is the heat flow from the SF obtained from the simulation with Equation (9), where $\dot{m}$ is the current total mass flow, c_p the heat capacity and T_{out} and T_{in} the outlet and inlet temperature of the HTF, respectively.

$$\dot{Q} = \dot{m}c_p(T_{out} - T_{in}) \tag{9}$$

The power block is represented by an efficiency matrix with variables HTF mass flow and HTF inlet temperature to the heat exchanger. A constant ambient temperature of 25 °C is used for the cooling end in this simplified power block model. Fig. 10 illustrates the efficiency matrix. The efficiency η_{PB} ranges from 32 % at 110 kg/s and 400 °C to 43 % at 350 kg/s and 505 °C. The efficiency curve is generated from a detailed heat flow diagram for a molten salt power block. The efficiency of power blocks in CSP is presented in papers [30] and [31]. The efficiencies described in these papers are in the range used in this paper. The HTF is not used for power generation when the solar field outlet temperature drops below 397.5 °C. It is assumed that in this case the HTF is returned to the cold tank. In the same way, the power consumption of the PB P_{PB} is calculated, see Fig. 11. The power consumption of the PB P_{PB} ranges from 0.7 MW at 110 kg/s and 440 °C to 1.7 MW at 350 kg/s and 505 °C. For lower temperature than 440 °C it is assumed, that the power consumption is the same as at 440 °C.

The power consumption of the main HTF pump is calculated with Equation (10), where $\dot{V}$ is the volume flow, Δp the pressure difference at the pump and η_{pump} the efficiency of the pump, here estimated to be 80 %.

$$P_{pump} = \frac{\dot{V}\Delta p}{\eta_{pump}}\left(\frac{\dot{m}}{\dot{m}_{max}}\right)^2 \tag{10}$$

For the calculation of the total generated electrical energy the integral of the difference between the heat flow $\dot{Q}$ multiplied with the efficiency of the PB η_{PB} and the power consumption of the PB P_{PB} and of the HTF pump P_{pump} is formed (Equation (11)

$$E_{net} = \int \dot{Q}(t)\eta_{PB}(t) - P_{PB}(t) - P_{pump}(t)dt \tag{11}$$

This value is available for each simulated day and used in averaged form over all simulated days. In addition to this energetic performance indicator further technical aspects, such as the average outlet temperature or the focus rate are considered.

Soiling of the collectors.

A real SF is never completely clean. Sequential cleaning furthermore leads to an inhomogeneous soiling situation across the field. It is expected that individual loop valve control can better adapt to spatially inhomogeneous heat inputs. A soiling condition test setup is defined for the simulation studies to investigate the performance of both control concepts under such circumstances.

A loop-individual cleanliness factor is used in the simulation to represent different soiling conditions across the field. Following [32] a simple soiling simulator was implemented. Starting with clean collectors a soiling rate in form of a normal distribution with a mean value of 0.5 %

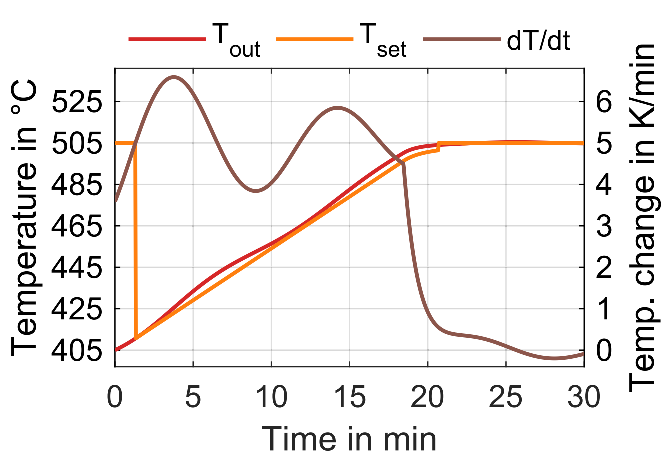

Fig. 9. Example of the trajectory control of the temperature gradient.

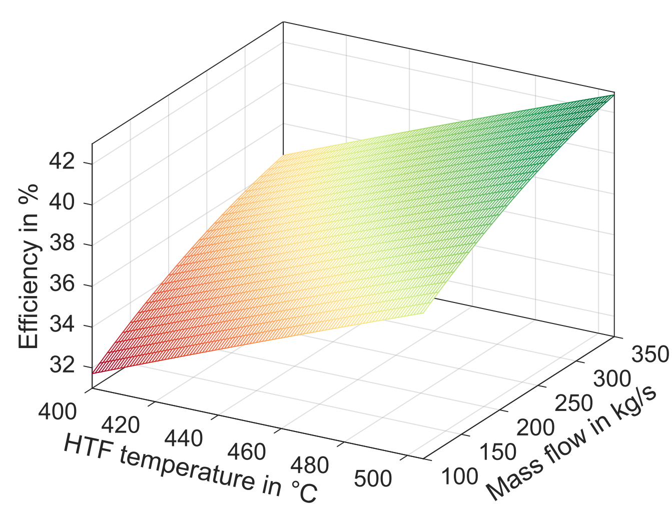

Fig. 10. Efficiency of the PB depending on HTF temperature and mass flow.

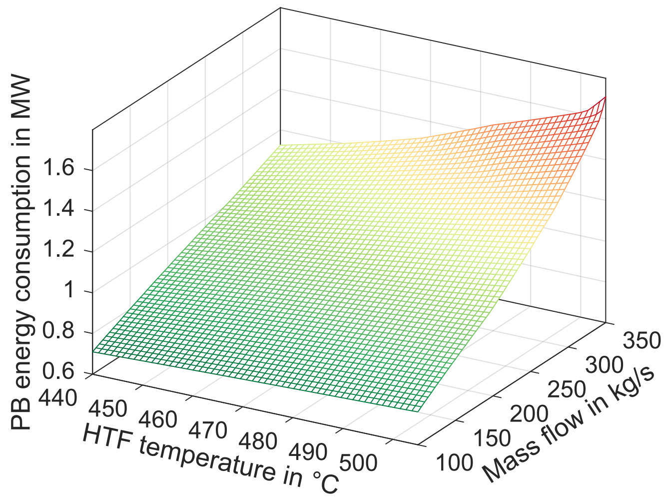

Fig. 11. Power consumption of the PB depending on HTF temperature and mass flow.

per day and a standard deviation of 0.2 % per day is implemented. These parameters represent average soiling situations at CIEMAT's PSA [33]. The daily soiling over the SF is assumed homogenous. Three loops per day are cleaned in succession as soon as the average field cleanliness drops below 97 %. A histogram of an average distribution of the cleanliness between the loops, which is used for the evaluation, is shown in Fig. 12 (left). To show the effects in more extreme situations, a setup with a mean of 1.6 % per day and a standard deviation of 0.6 % per day is used [34]. Also a sand storm was stimulated with a sudden soiling rate of 20 % in one single day [35]. Fig. 12 (middle) shows an average cleanliness situation for the sand desert and Fig. 12 (right) the soiling situation after five days of cleaning (15 cleaned loops) after a sand storm.

The soiling condition values as illustrated in Fig. 12 are implemented as constant throughout the simulation. In VSF, an individual cleanliness factor is specified for a loop. This factor lies between 0 and 1 and can thus influence the absorbed energy in the loop. The factor can be specified individually for each loop.

3. Simulation results

The two controller setups with/without individual loop control valves are compared to each other. The first step is the technical comparison of the controllers. In the second step, the controllers are evaluated under inhomogeneous heat inputs.

3.1. Comparison of controller performance at example days

The technical comparison aims to analyze the performance differences between the two control concepts in terms of focusing, mass flow and temperature. For this investigation, it is assumed that all collectors have equal cleanliness of 100 %. In the first step, the two concepts are analyzed for a day with clear sky conditions. These conditions are characterized by a homogeneous heat input over the solar field resulting in a default mass flow distribution. Valve openings should therefore only deviate within the inaccuracy of the positioner from the default opening.

Fig. 13 displays the simulation results for a day with stable DNI conditions. The outlet temperature and the SF focusing of the two control concepts are presented. The mass flow for the control concept with equal mass flow distribution and the minimum and maximum mass flow in the loops for the control valve concept are shown. Minimum and maximum mass flows in the SF are nearly identical for the valve controller. This indicates that the valves are close to their base opening without large fluctuations. The mean value of the mass flow controller is used as a comparison for temperature and focusing, and the differences to the valve controller are given as a percentage deviation. In this scenario, the differences are very small at 0.18 % for temperature and 0.02 % for focusing, which is due to the homogeneous irradiation and therefore the same conditions throughout the SF. A deviation of 1.02 K from the setpoint temperature of 505 °C was achieved for the valve controller, while a deviation of 1.94 K was achieved for the reference controller.

In a second step, the control concepts are analyzed under transient irradiation conditions. Fig. 14 shows for the effective irradiation under a partly cloudy situation starting at around 12o'clock. This leads to spatio-temporal fluctuations of DNI over the SF. These are seen in the figure as average in solar irradiation over the SF. In the periods from approximately 13:00 to 13:10 and 14:45 to 15:00, the irradiation falls to a low level. For both control systems the minimum mass flow limit is reached. The mass flow limited to the minimum mass flow is still too high to keep the temperature at the setpoint. As a result, the outlet temperature drops during this period. During the other periods between 12:00 and 16:00, the valve control concept sets individual mass flows in the loops (to be seen by the min and max values given in the plot). The focus rate is very stable close to the ideal value of 100 %. The field outlet temperature is closer to 505 °C than in the mass flow control concept. In absolute values, the average loop outlet temperature is 4.44 K higher and the average focus rate is 0.79 %-points higher in this period.

The impact of the minimum mass flow restriction is illustrated in Fig. 15 which shows a typical winter day with low irradiation. The day has a cloudy situation at the beginning and clear sky situation from 13:00 on. Due to the low irradiation, both control concepts fall to minimum mass flow. Design outlet temperatures are not reached for this mass flow since the irradiation level is too low. The performance of both control concepts does not deviate much since the field is operated by minimum mass flow anyway. Besides the controller performance, the example illustrates the importance of bringing down the minimum mass flow in order to reach outlet temperature also under these conditions.

3.2. Annual performance under clean collector condition

Simulation runs with the individual ASI-based irradiation profiles (spatial and temporal) as introduced in section 3.1 are executed for all available days over the three years. The valve control concept is compared to the fix valve control concept in terms of difference in electric energy produced. Fig. 16 shows the monthly absolute and relative change in the net electrical energy produced per month. The

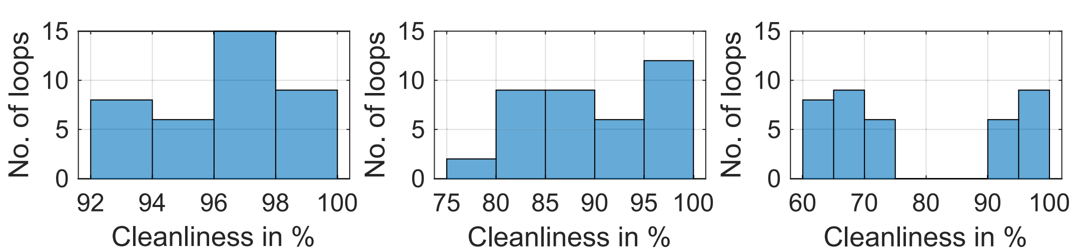

Fig. 12. Cleanliness distribution of the 38 loops under normal soiling conditions (left), sand desert conditions (middle), and harsh sand storm conditions (right).

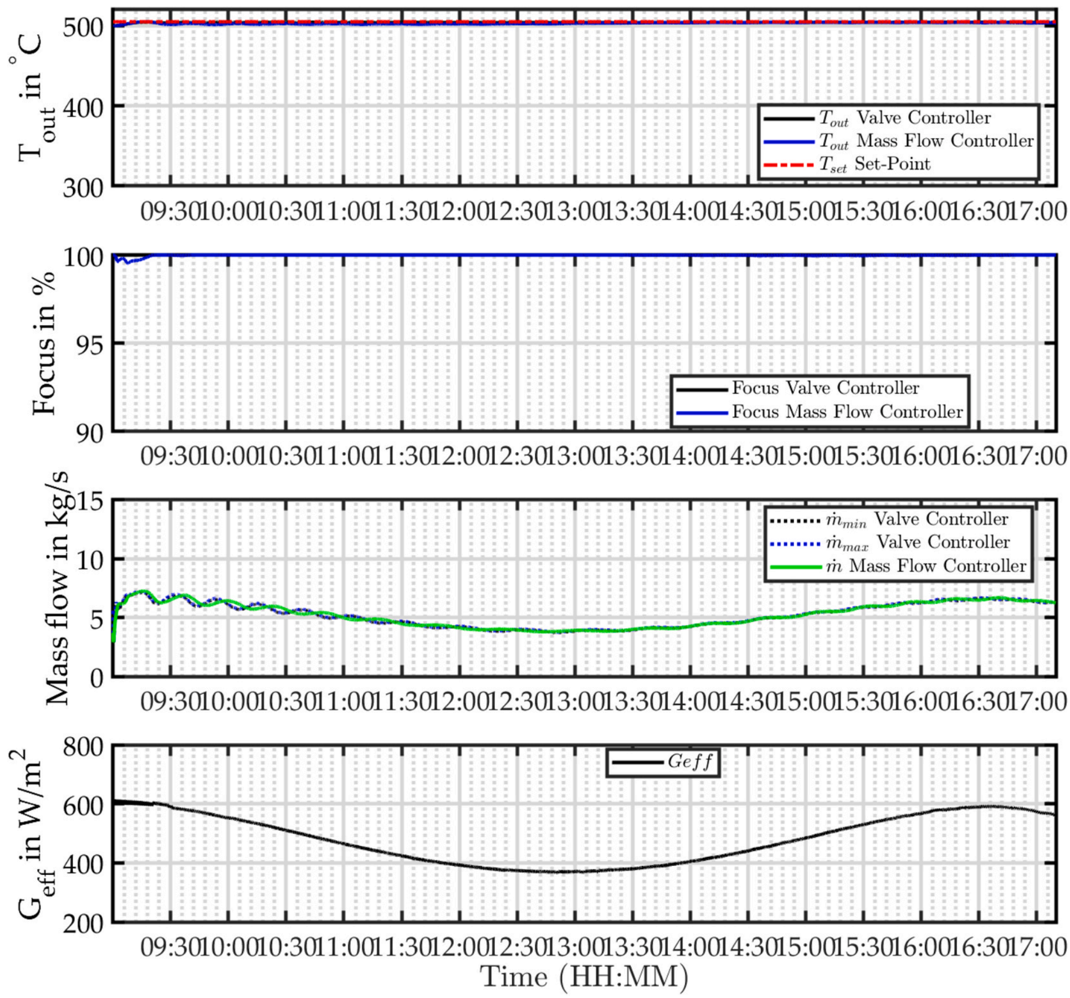

Fig. 13. Simulated controller performance for a clear sky day expressed in terms of solar field outlet temperature, average of collector focus, minimum/maximum value of loop mass flows for valve controller and average loop mass flow for mass flow controller (26.10.2017).

change ranges from −1.4 MWh/month or −0.1 % in November 2016 to + 150 MWh/month or + 2.2 % in May 2018. On average over the three-year period, the HTF outlet temperature is 1.6 K higher and the HTF mass flow is 1.3 kg/s lower with the valve control concept compared to the control concept without loop-wise control valves. The average focus rate is 0.27 % higher than with fixed valve control. In total, the net electrical energy produced is increased by 0.57 % or 1235 MWh (396 MWh in 2016, 289 MWh in 2017 and 550 MWh in 2018). There is almost no difference throughout the winter months since minimum mass flow conditions are often reached There are also differences in the control concepts for situations with transient conditions, such as cloud cover. As the reduced irradiation in cloudy conditions also results in a lower yield, the advantage of the control valves in the cumulative results is small.

3.3. Annual performance under soiled collector conditions

In a real solar field, the collectors are usually inhomogeneously soiled due to cleaning cycles of typically 7 to 14 days. The fixed valve control concept is not able to adapt to different soiling conditions in the loop. Instead, either the SCAs in average are slightly defocused or the average outlet temperature does not reach its nominal value. These two approaches must be combined in the best possible way to generate as much net electrical energy as possible. The individual valve control concept has additional degree of freedom by adjusting the loop control valves. This therefore represents the real behavior of the power plant, as the mass flow distribution with manual valves deviates from the optimal distribution with homogeneous irradiation. It tests an average normal soling, as can be found at a power plant site in Spain. The cleanliness ranges from 92 % to 100 %. A histogram of the cleanliness distribution is shown in Fig. 12 (left).

Fig. 17 shows the increase in absolute and relative net electrical energy produced, from + 0.4 MWh/month or + 0.0 % in December 2016 to + 156 MWh/month or + 2.3 % in June and May 2018, respectively. Overall, the average HTF outlet temperature increased by 2.8 K and the average HTF mass flow rate decreased by 2.5 kg/s, with the focus rate increasing by 0.42 %. Over the three-year period, an increase of 0.85 % or 1,761 MWh (552 MWh in 2016, 512 MWh in 2017 and 697 MWh in 2018) of net generated electrical energy was achieved. The result is quite similar to that of the clean collectors, but with a higher overall efficiency of the power plant and a higher increase in net electrical energy generated per month.

The additional net electric energy production when using the loop valve control concept is 587 MWh/year in average for normal soiling conditions. Applying in an auction price of 0.076 USD/kWh [36], this additional electric energy translates to a monetary benefit of 44,612 USD/year. With assumed additional cost for motorized and controlled valves of 10,000 USD/loop, the investment is covered after 8.5 years under the normal soiling conditions. Additional savings result from reduced man power for hydraulic field balancing during commissioning and for subsequent re-balancing during operation. This study does not evaluate the additional benefits of reduced maintenance

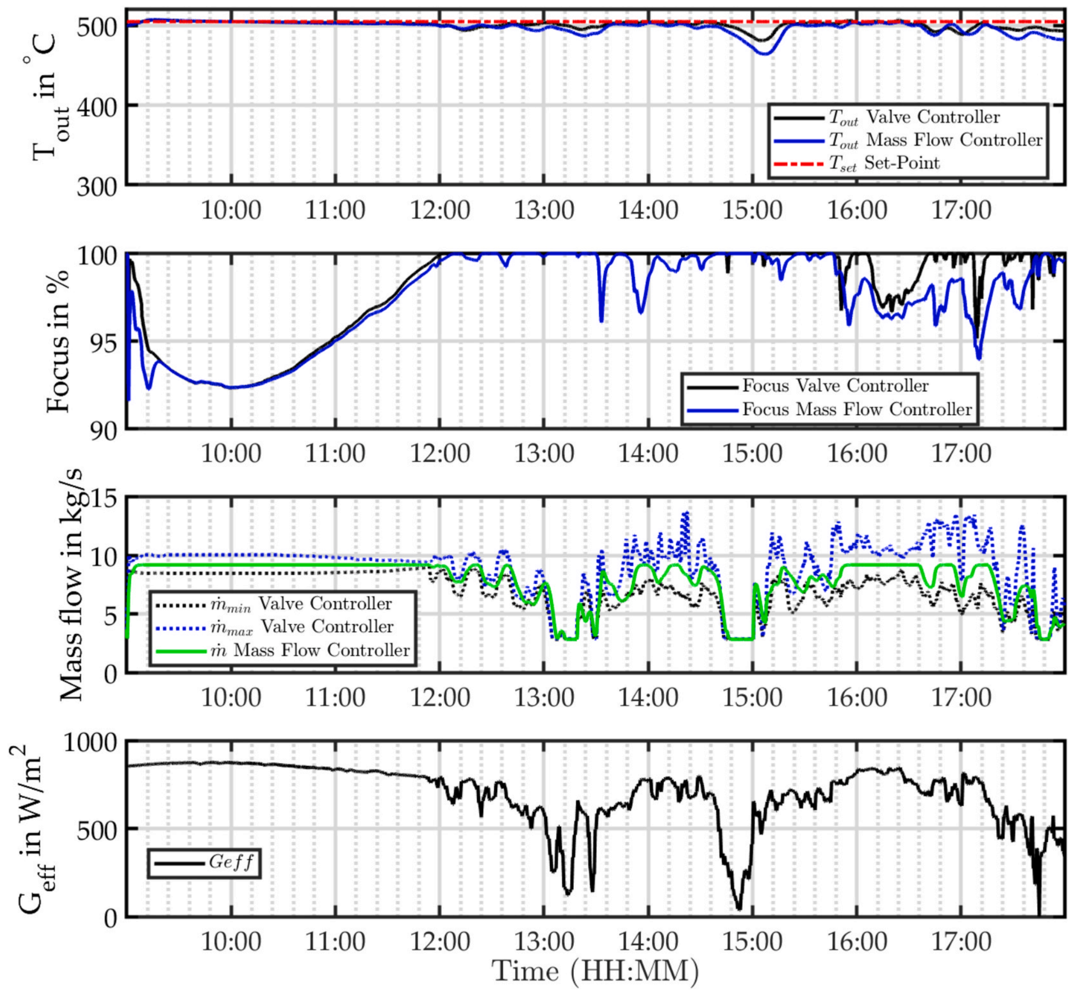

Fig. 14. Simulated controller performance for a day with non-stable irradiance conditions (16.04.2016).

due to substantially reduced temperature gradients at the loop ends and in the collecting header lines.

3.4. Annual performance under extreme soiling situations

Controller performance under larger differences in spatial soiling distribution over the field are now investigated. Two test setups as described in section 2.3 are used. On the one hand, soiling under sand desert conditions is analyzed and, on the other hand, the behavior of the SF is tested for a few days after a sand storm where a part of the rather dirty field has already undergone cleaning.

Sand desert conditions.

The highest permanent soiling rates are found in sand deserts. An average soiling situation is shown in Fig. 12 (middle), with cleanliness of the collectors ranging between 75 % und 100 %. Fig. 18 shows the monthly absolute and relative change in net electrical energy produced in the sand desert regime. The benefit of the valve controller compared to the fix controller ranges from −0.9 MWh/month or −0.1 % in December 2018 and December 2016 to + 338 MWh/month or + 3.9 % in June and May 2018. With individual valve control, the average HTF outlet temperature is 5.9 K higher, the average HTF mass flow is 4.2 kg/s lower and the average focus rate is 1.24 % higher. Over the three-year period, an increase of 2.63 % or 5012 MWh (1550 MWh in 2016, 1798 MWh in 2017 and 1,665 MWh in 2018) of net generated electrical energy was achieved. Compared to the benefits obtained under normal soiling conditions, see Fig. 17, the benefit of the individual valve control concept is about 3 times higher. This illustrates the potential of the individual valve control especially under the strongly inhomogeneous soiling conditions.

Post sand storm conditions.

This test setup shall provoke a condition with large differences in soiling between the loops resulting from strong soiling after a sand storm combined with a fraction of the loops already cleaned. Only one representative day – 5 days after the sand storm – is evaluated. A histogram of the resulting cleanliness of the SCAs used for this analysis is shown in Fig. 12 (right). 23 SCAs have a cleanliness between 60 % and 75 % and 15 SCAs show a cleanliness of 90 % or more. Fig. 19 shows the mean, minimum and maximum irradiation for the selected day (19.06.2016). Most of the time, the DNI is almost stable between 800 W/m^2 and 900 W/m^2. At 11:00 a cloud event reduces the mean DNI to about 500 W/m^2 for 45 min.

Fig. 20 shows the average HTF outlet temperature over all loops and average focus rate during the day. For the fixed valve control concept (left), the nominal HTF outlet temperature of 505 °C cannot be reached. The average focus rate of ∼ 92 % (due to the focus reduction of the cleaner loops) and the average temperature of ∼ 485 °C indicates the trade-off the fixed valve control concept has to accept. Cleaner loops have to be partially defocused to avoid over-temperatures whereas dirty loops do not reach the outlet temperature although all collectors are in full track. The fixed valve control concept could be further trimmed to set priority in reaching either higher outlet temperature (by further reducing mass flow and increasing focusing) or higher focus rate (by increasing mass flow and reducing average outlet temperature) Individual valve control can compensate for these differences in cleanliness

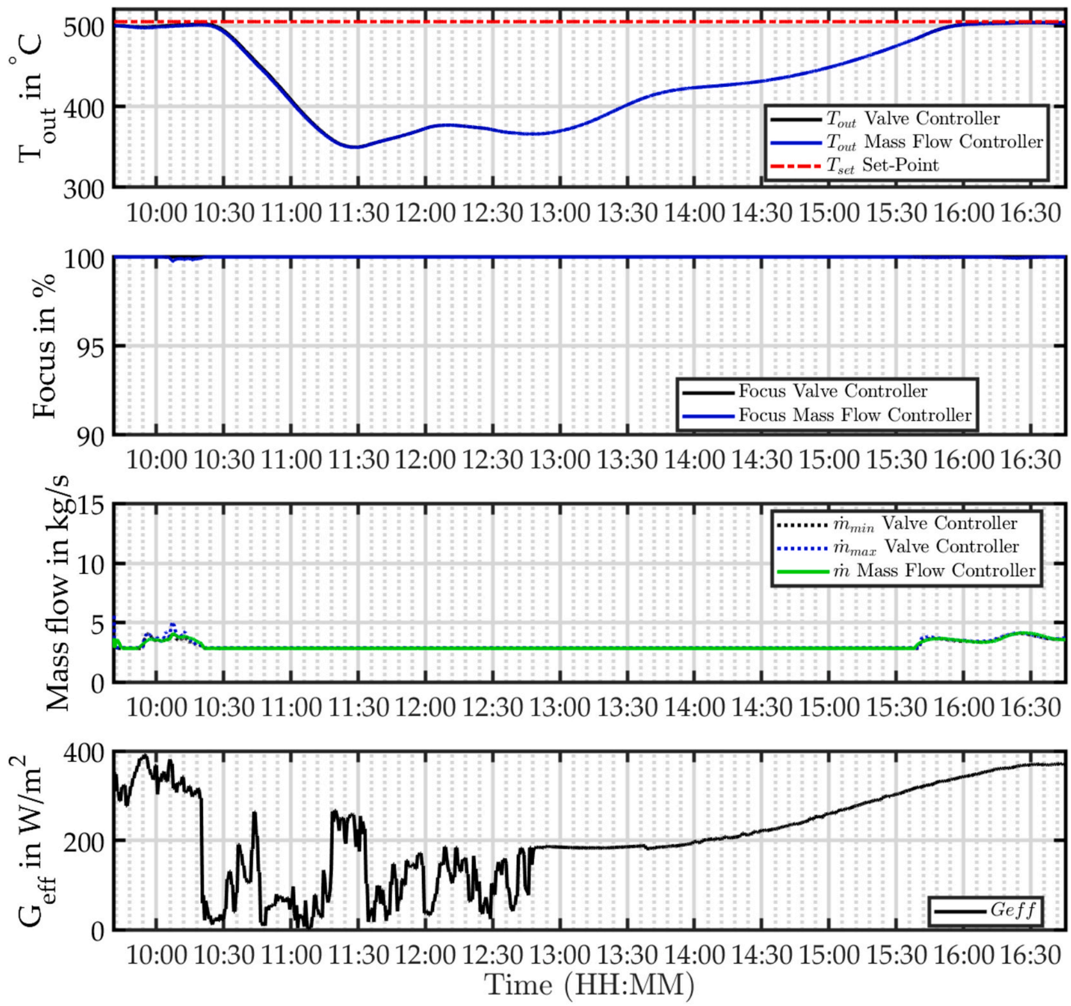

Fig. 15. Simulated controller performance for a winter day (02.01.2016). Since minimum mass flow limitation is reached outlet temperature, mass flow and focus rate of the two control concepts are identical over long periods.

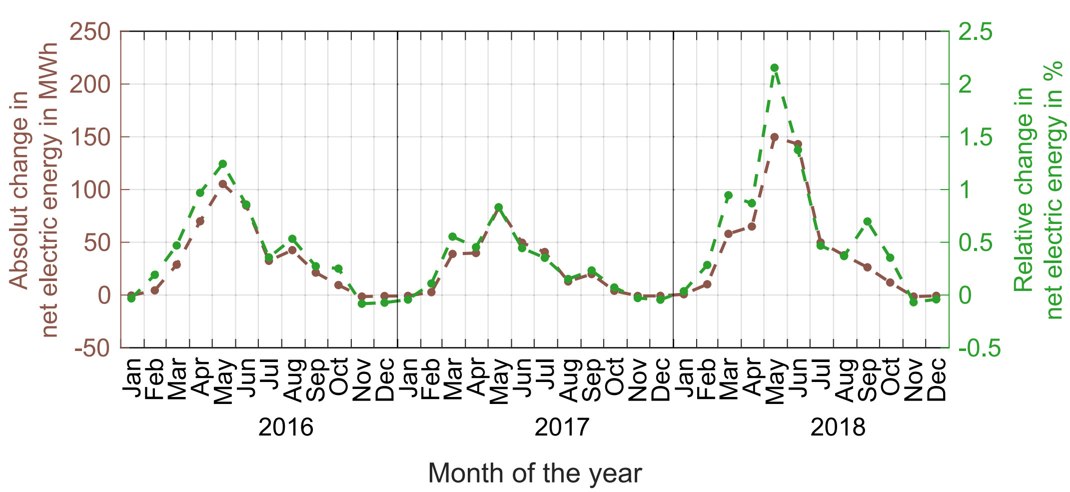

Fig. 16. Monthly mean absolute (brown) and relative (green) change in monthly net electrical energy of the individual valve control compared to the fixed valve control for clean SCAs.

in a much better way. The focus rate is almost 100 %, the HTF mass flow to the field is 5.6 kg/s higher, and the average loop outlet temperature is 18.5 K higher. Overall, the net electrical energy produced increases by 15.2 % or 46.5 MWh for this specific day. According to the price assumptions from chapter 3.3 of 0.076 USD/kWh, an added value of 3,534 USD/loop can be generated in this situation. However, it should be noted that the sandstorm does not occur regularly and the calculation is based on this one day. The efficiency of cleaning the solar field after a

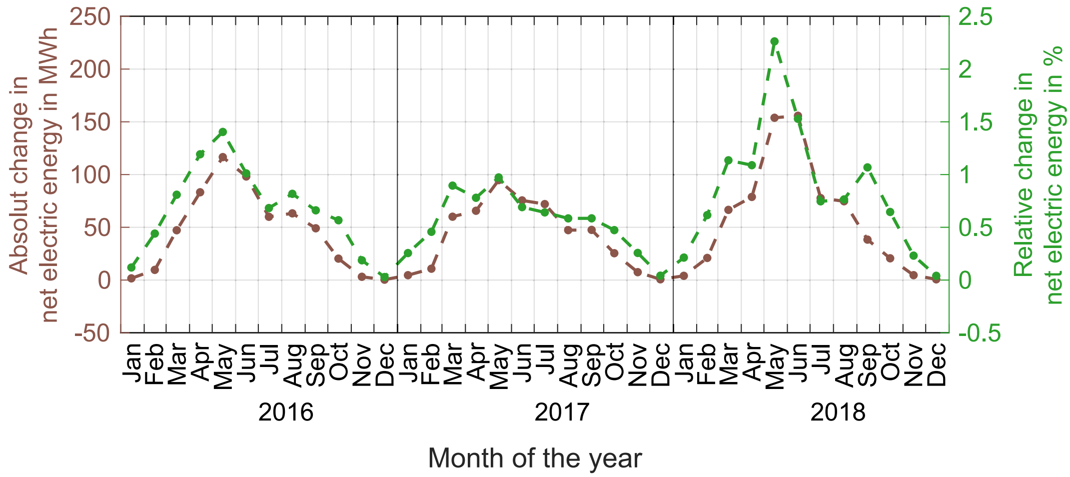

Fig. 17. Monthly mean absolute (brown) and relative (green) change in monthly net electrical energy of the individual valve control compared to the fixed valve control for normally soiled SCAs according to Fig. 12.

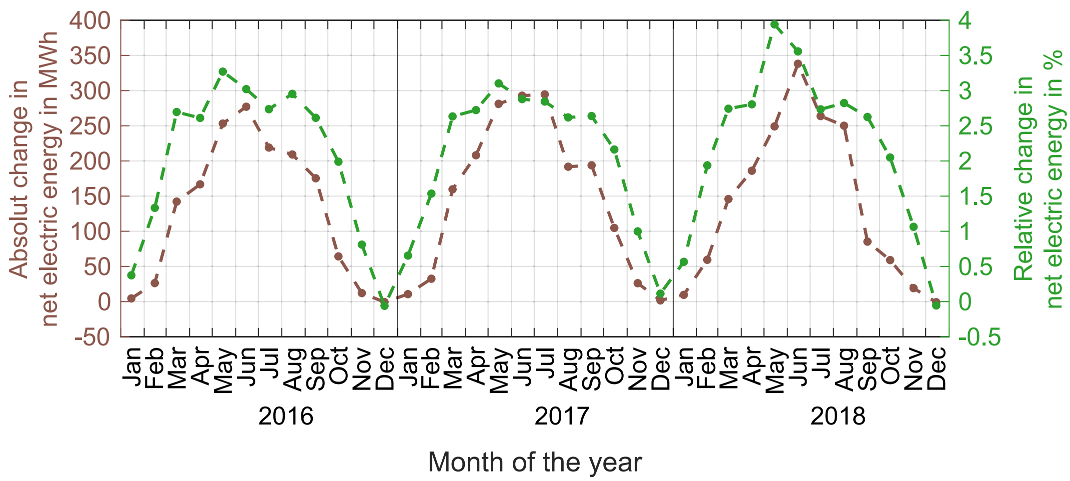

Fig. 18. Monthly mean absolute (brown) and relative (green) change in monthly net electrical energy of the individual valve control compared to the fixed valve control for SCAs in sand desert conditions.

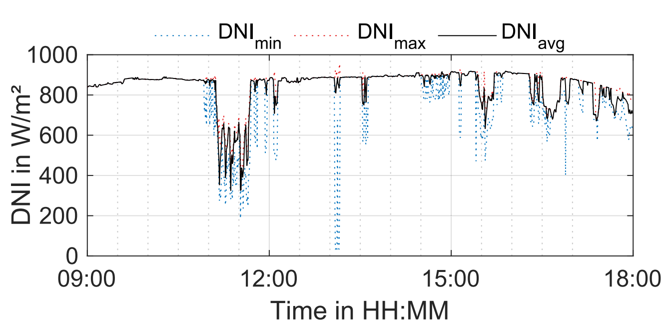

Fig. 19. Irradiation conditions for the example day June 19, 2016 used for the sand storm condition test.

sandstorm is a crucial factor here. Since clear sky and cloudy conditions are mixed on that day, the results represent the overall benefit of the loop control concept under uneven soiling and uneven irradiation.

4. Conclusion

The paper presents a numerical study for the flow control of a parabolic trough solar field using individual loop control valves. The performance is compared to a control concept with fixed loop valves. As part of this work, both the control system with control valves and the control system with fixed loop valves were developed and compared. The simulations are executed by the detailed transient simulation tool VSF. A total of 940 operation days recorded at CIEMAT's PSA is simulated using DNI maps collected by an all sky imager system operated over a three year period. In addition to the spatio-temporal inhomogeneity of the irradiance conditions, uneven soiling conditions over the field are used as test cases. The scenarios range from clean, normally soiled, heavily soiled (sand desert) and extremely soiled (sand storm) collectors. The valve control concept is evaluated by the daily amount of electric energy produced, the stability of the average loop outlet temperature, the average focus rate, and the mass flow in the field.

Evaluation over the 940 days show that the net electrical energy produced can be increased by 0.57 % (clean collectors), 0.85 % (normally soiled), 2.63 % (heavily soiled) and 15.2 % (extremely soiled) conditions. The average outlet temperatures can also be increased by 1.6 K, 2.8 K, 5.9 K, and 18.5 K, respectively. The results show an improvement of the developed control system with control valves compared to the developed control system with fixed valves.

Example days are used to illustrate the performance of the two control concepts presented in this paper under different irradiation

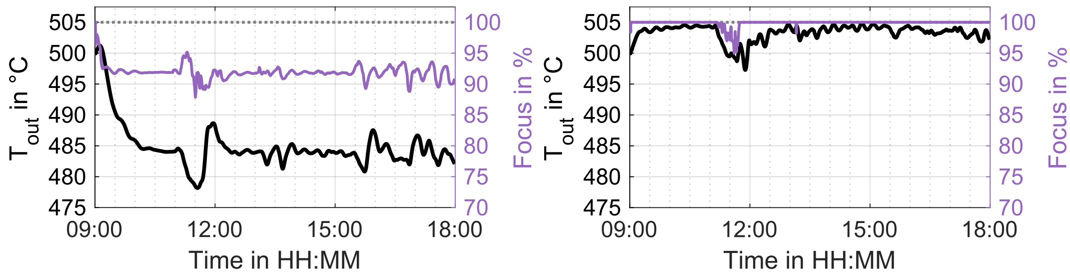

Fig. 20. Average loop outlet temperature and focus rate on 19.06.2016 with fixed valve control (left) and individual valve control (right) under post sand storm conditions as defined in section 2.3.

conditions. During periods of homogeneous irradiation, well-balanced fix valve settings lead to nearly an ideal mass flow distribution which is required to reach the desired loop outlet temperatures. Transient irradiance conditions, such as induced by clouds, lead to inhomogeneous heat input over the loops. The constant mass flow distribution leads to variations in the outlet temperatures, reduced focus rate, and in consequence for reduced energy generation. The control concept with individual control valves is able to keep the outlet temperature and focus in the solar field closer to the setpoint. Simulation results also reveal the relevance of the minimum mass flow limitation. As soon as the minimum mass flow is reached, the desired loop outlet temperature can no longer be achieved. Such situations typically occur during winter days. Simulation results assuming unevenly soiled collector loops clearly show the strength of the individual loop valve control concept. The mass flow in each loop can be adjusted to the current soiling conditions bringing the outlet temperature close to the design value.

It can be assumed that, in the event of normal soiling, an increased electrical energy production of 587 MWh/year could be achieved, which would correspond to an increase of 44,612 USD/year. Consequently, the control valves investment is covered after 8.5 years. When the loop valve control is used under sand desert scenario, the value is increases to 126,978 USD/year.

The results of the presented detailed simulation study clearly reveal the potential of individual loop control valves for the example case of a molten salt parabolic trough field with 38 loops. Future work should include optimized control approaches for the start-up, shut-down, anti-freeze, and recirculation modes. Determination of the controller parameters from the solar field characteristics could be automatized in order to reduce efforts in tuning the controllers. The presented investigation assumed constant solar field inlet temperatures. The impact of varying inlet temperatures could be cross-checked although the impact on the benefits of loop wise control are expected be small. The same holds true for the size of the solar field. It is not expected that the relative benefits are significantly influenced by the field size itself, since the benefit results from the extent of inhomogeneities over the field, but not the size of the field.

CRediT authorship contribution statement

Tim Kotzab: Writing – review & editing, Writing – original draft, Software, Methodology, Formal analysis, Conceptualization. **Sebastian Müllner:** Writing – review & editing, Writing – original draft, Methodology. **Jana Stengler:** Writing – review & editing. **Bijan Nouri:** Writing – review & editing. **Luis Fernando Zarzalejo:** Writing – review & editing. **Mark Schmitz:** Writing – review & editing. **Tobias Hirsch:** Writing – review & editing, Methodology.

Declaration of Competing Interest

The authors declare that they have no known competing financial interests or personal relationships that could have appeared to influence the work reported in this paper.

Acknowledgments

Funding was received by the German Federal Ministry for Economic Affairs and Energy within the MSOpera project (Grant Agreement 03EE5028B).

Thanks to the colleagues from the Solar Concentrating Systems Unit of CIEMAT for the support provided in the installation and maintenance of the shadow cameras. These instruments are installed on CIEMAT's CESA-I tower of the Plataforma Solar de Almería.

References

[1] IRENA, "Renewable capacity statistics 2021," International Renewable Energy Agency (IRENA), Abu Dhabi, 2021a.
[2] M.T. Islam, N. Huda, A.B. Abdullah, R. Saidur, A comprehensive review of state-of-the-art concentrating solar power (CSP) technologies: Current status and research trends, *Renew. Sustain. Energy Rev.* 91 (2018) 987–1018, https://doi.org/10.1016/j.rser.2018.04.097.
[3] NREL. "Lebrija 1 CSP Project." Accessed: Mar. 2, 2025. [Online]. Available: https://solarpaces.nrel.gov/project/lebrija-1.
[4] NREL. "Archimede CSP Project." Accessed: Mar. 2, 2025. [Online]. Available: https://solarpaces.nrel.gov/project/archimede.
[5] E.F. Camacho, F.R. Rubio, M. Berenguel, L. Valenzuela, A survey on control schemes for distributed solar collector fields. Part I: Modeling and basic control approaches, *Sol. Energy* 81 (10) (2007) 1240–1251, https://doi.org/10.1016/j.solener.2007.01.002.
[6] E.F. Camacho, F.R. Rubio, M. Berenguel, L. Valenzuela, A survey on control schemes for distributed solar collector fields. Part II: Advanced control approaches, *Sol. Energy* 81 (10) (2007) 1252–1272, https://doi.org/10.1016/j.solener.2007.01.001.
[7] M. Barão, J.M. Lemos, R.N. Silva, Reduced complexity adaptive nonlinear control of a distributed collector solar field, *J. Process Control* 12 (1) (2002) 131–141, https://doi.org/10.1016/S0959-1524(01)00003-8.
[8] A. Brenner, T. Hirsch, M. Röger, and R. Pitz-Paal, "State-of-the-Art Measurement Instrumentation and Most Recent Measurement Techniques for Parabolic Trough Collector Fields," *energies*, vol. 14, no. 21, 2021, doi: 10.3390/en14217166.
[9] T. Schlichting, "Bewertung der Verwendbarkeit von Strahlungskarten für den Einsatz in der Regelung eines Parabolrinnensystems," Masterthesis, U. Duisburg-Essen, 2018.
[10] S. Müllner, "Situationsangepasste Reglerparametrierung für Parabolrinnenkraftwerke," Masterthesis, Ostbayerische Technische Hochschule Regensburg, 2020.
[11] B. Nouri, et al., Optimization of parabolic trough power plant operations in variable irradiance conditions using all sky imagers, *Sol. Energy* 198 (2020) 434–453, https://doi.org/10.1016/j.solener.2020.01.045.
[12] T. Kotzab, et al., Parabolic trough field control utilizing all sky imager irradiance data – A comprehensive robustness analysis, *Sol. Energy* (2022).
[13] T.A. Johansen, K.J. Hunt, I. Petersen, Gain-Scheduled Control of a Solar Power Plant 8 (9) (2000) 1011–1022.
[14] E. F. Camacho and C. B. Alba, *Model Predictive Control*. Springer-Verlag, 2007.
[15] M. Berenguel, E.F. Camacho, F.R. Rubio, P.C.K. Luk, Incremental Fuzzy PI Control of a Solar Power Plant 144 (6) (1997) 596–604.
[16] J. Henriques, P. Gil, A. Cardoso, and A. Dourado, "Scheduling of PID controllers by means of a Neural Network With Application to a Solar Power Plant," vol. 1.
[17] A.J. Sánchez, A.J. Gallego, J.M. Escaño, E.F. Camacho, Temperature homogenization of a solar trough field for performance improvement, *Sol. Energy* 165 (2018) 1–9, https://doi.org/10.1016/j.solener.2018.03.001.
[18] A.J. Sánchez, A.J. Gallego, J.M. Escaño, E.F. Camacho, Thermal balance of large scale parabolic trough plants: A case study, *Sol. Energy* 190 (2019) 69–81, https://doi.org/10.1016/j.solener.2019.08.001.
[19] M. Abutayeh, et al., Effect of short cloud shading on the performance of parabolic trough solar power plants: motorized vs manual valves, *Renew. Energy* 142 (2019) 330–344, https://doi.org/10.1016/j.renene.2019.04.094.

[20] J.R.D. Frejo, E.F. Camacho, Centralized and distributed Model Predictive Control for the maximization of the thermal power of solar parabolic-trough plants, *Sol. Energy* 204 (2020) 190–199, https://doi.org/10.1016/j.solener.2020.04.033.

[21] E.F. Camacho, A.J. Gallego, Optimal operation in solar trough plants: A case study, *Sol. Energy* 95 (2013) 106–117, https://doi.org/10.1016/j.solener.2013.05.029.

[22] E. Masero, J.R.D. Frejo, J.M. Maestre, E.F. Camacho, A light clustering model predictive control approach to maximize thermal power in solar parabolic-trough plants, *Sol. Energy* 214 (2021) 531–541, https://doi.org/10.1016/j.solener.2020.11.056.

[23] M. Hasenbalg, P. Kuhn, S. Wilbert, B. Nouri, A. Kazantzidis, Benchmarking of six cloud segmentation algorithms for ground-based all-sky imagers, *Sol. Energy* 201 (2020) 596–614.

[24] P. Kuhn, et al., Validation of an all-sky imager-based nowcasting system for industrial PV plants, *Prog. Photovolt. Res. Appl.* 26 (8) (2018) 608–621, https://doi.org/10.1002/pip.2968.

[25] B. Nouri, et al., Cloud height and tracking accuracy of three all sky imager systems for individual clouds, *Sol. Energy* 177 (2019) 213–228.

[26] B. Nouri, et al., Real-Time Uncertainty Specification of All Sky Imager Derived Irradiance Nowcasts, *Remote Sens. (basel)* (2019).

[27] K. Noureldin, “Modellierung und Regelung transienten Verfahren in Parabolrinnenkraftwerke mit einphasigem Wärmeträgermedium,” Rheinisch-Westfälischen Technischen Hochschule Aachen, 2018.

[28] K. Noureldin, T. Hirsch, R. Pitz-Paal, Virtual Solar Field - Validation of a detailed transient simulation tool for line focus STE fields with single phase heat transfer fluid, *Sol. Energy* 146 (2017) 131–140, https://doi.org/10.1016/j.solener.2017.02.028.

[29] K.-J. Riffelmann *et al.,* “HELIOTROUGH–A new collector generation for parabolic trough power plants,”.

[30] T. Lopes, T. Fasquelle, H.G. Silva, Pressure drops, heat transfer coefficient, costs and power block design for direct storage parabolic trough power plants running molten salts, *Renew. Energy* 163 (2021) 530–543, https://doi.org/10.1016/j.renene.2020.07.110.

[31] H. Yan, A. Wang, D. Chong, M. Liu, J. Liu, and J. Yan, “Review on Performance Analysis of the Power Block in Concentrated Solar Power Plants,” *Energy Tech*, vol. 9, no. 1, 2021, Art. no. 2000621, doi: 10.1002/ente.202000621.

[32] S. Horstmann, “Online Optimization - Cleaning strategies for CSP plants,” Faculty of Mathematics and Natural Sciences, U. o. Cologne, 2021.

[33] F. Wolfertstetter *et al.,* “Modelling the soiling rate: Dependencies on meteorological parameters,” in 2019, doi: 10.1063/1.5117715.

[34] F. Wolfertstetter, et al., Monitoring of Mirror and Sensor Soiling with TraCS for Improved Quality of Ground based Irradiance Measurements, *Energy Procedia* 49 (2014) 2422–2432, https://doi.org/10.1016/j.egypro.2014.03.257.

[35] F. Wolfertstetter, S. Wilbert, J. Dersch, S. Dieckmann, R. Pitz-Paal, and A. Ghennioui, “Integration of Soiling-Rate Measurements and Cleaning Strategies in Yield Analysis of Parabolic Trough Plants,” *Journal of Solar Energy Engineering*, vol. 140, no. 4, 2018, doi: 10.1115/1.4039631.

[36] IRENA, “Renewable Power Generation Costs in 2020,” International Renewable Energy Agency (IRENA), Abu Dhabi, 2021b.